

Strain effects on insulator-to-metal transition and electronic structure in VO₂

S. R. Sahu,^{1,*} S. S. Majid^{2,*} A. Tripathy,¹ N. Bano,¹ A. Ahad³,^{Hyungwoo Lee}^{4,5} V. G. Sathe,¹ and D. K. Shukla^{1,†}

¹UGC-DAE Consortium for Scientific Research, Indore 452001, India

²Department of Physics, National Institute of Technology Hazratbal Srinagar J & K-190006, India

³School of Physical and Mathematical Sciences, Nanyang Technological University, 637371, Singapore

⁴Department of Physics, Ajou University, Suwon 16499, Republic of Korea

⁵Department of Energy Systems Research, Ajou University, Suwon 16499, Republic of Korea

 (Received 18 December 2023; revised 15 February 2024; accepted 22 March 2024; published 10 April 2024)

Tunability of near-room temperature insulator-to-metal transition (IMT) of VO₂ is a prerequisite for its applications in switching and sensing devices. IMT in VO₂ is accompanied with structural transition, monoclinic (insulating) to rutile (metallic), where the V-V dimer of the monoclinic phase becomes equidistant in the rutile phase. Tuning of the V-V dimer distances can result in dramatic changes in IMT characteristics. However, understanding of such processes has been limited due to intrigued relations between structure, electronic structure, and IMT of VO₂. By utilizing the substrate and Cr doping-induced strain, we have grown VO₂ thin films with distinct V-V dimers, which has enabled us to study the effect of these dimers on the structure, IMT, and electronic structures of VO₂. In addition to the usual *M1* phase of VO₂, strain-mediated *T* and *M2* phases have been stabilized with the help of both Cr doping and tensile strain along the *c_R* axis. We have observed that a small compressive strain ($\approx 0.19\%$) along the *c_R* axis (\approx monoclinic *a_M* axis) lowers the transition temperature significantly (by $\approx 10^\circ\text{C}$) compared to bulk. Temperature-dependent Raman spectroscopy measurement is used to track the exact structural transformation route followed by these insulating phases of VO₂. Dependent on the nature of strain along the *c_R* axis, IMT temperature is found to vary—increases (for tensile) or decreases (for compressive)—while Cr doping-induced strain has a less significant impact on the IMT temperature compared to the nature of the strain. X-ray absorption near-edge spectroscopy (XANES) has been utilized to examine the electronic structure of the grown VO₂ thin films. Temperature variation of pre-edge features (vanadium 3*d* orbitals) in XANES directly scales with the insulator-to-metal transition, which suggests that the electronic structure of VO₂ is strongly influenced by the nature (compressive/tensile) of strain, whereas minimal changes in electronic structure have been observed due to different insulating phases (*M1*, *T*, and *M2*). Our study underscores the important role of the nature of strain in tailoring the IMT in VO₂.

DOI: [10.1103/PhysRevB.109.155132](https://doi.org/10.1103/PhysRevB.109.155132)

I. INTRODUCTION

Vanadium dioxide (VO₂) is well known for its near-room-temperature ($\sim 67^\circ\text{C}$) insulator-to-metal transition (IMT) with a dramatic change in its electrical conductivity. IMT in VO₂ is accompanied by a first-order structural phase transition (SPT) from a low-temperature insulating monoclinic *M1* phase (*P2₁/c*) to high-temperature metallic rutile *R* phase (*P4₂/mnm*) [1,2]. VO₂ distinguishes itself from other phase change materials with its intrinsically coupled electronic and structural phase transition, which has made it a topic of classic debate for last ~ 60 yr: whether IMT in VO₂ is an electron-lattice interaction-driven Peierls type or an electron-electron interaction-driven Mott type. IMT in VO₂ can be tuned by external factors such as heat, electric field, doping, oxygen vacancy, and photons [3–11], which makes it suitable for novel technological applications such as smart windows, transistors, ultrafast switches, gas sensors, etc. [12–19].

While the bulk VO₂ exhibits only the *R* and the *M1* lattice structures, two additional lattice structures, monoclinic *M2* (*C2/m*) and triclinic *T* (*C $\bar{1}$*), can be accessed by chemical doping [20], tensile strain along *c_R* [21], and compressive strain along (110)_{*R*} [22]. For a complete understanding of the IMT mechanism in VO₂, one necessarily needs to combine the study of all four phases (*M1*, *M2*, *T*, and *R* phases), as their lattices are nearly similar. The insulating phases (*M1*, *M2*, *T*) exhibit different V-V pairing, and earlier studies suggest that the electronic structure of these insulating phases is essentially same, i.e., the electronic structure is insensitive to changes in the V-V pairing [23–26]. However, remarkable changes in the electronic structure and transition temperature have been observed with compressive strain along the *c_R* axis [27]. As a noticeable change in the V-V pairing in different insulating phases, a different V-V pairing distance has been also observed due to compressive or tensile strain along the *c_R* axis [28]. Moreover, it has been demonstrated that IMT in VO₂ largely depends on orbital occupancies [29]. Some literature also shows decoupling of transition temperatures of transitions in electronic structure and in electrical resistivity [6,30]. All these observations clearly indicate an intriguing

*These authors contributed equally to this work.

†dkshukla@csr.res.in

relationship between strain, V-V dimer distances, electronic structure, and IMT in VO₂.

The solution to such questions is concealed in the relationship between V-V dimer distances and its relation to electronic properties of VO₂. To address these issues, we have performed a comprehensive study on the effect of different V-V pairing arrangements on the IMT and electronic structure. Thin film samples have been utilized with the variants of compressive as well as tensile strains along the V-V pairing arrangement. We have grown pure and the Cr-doped VO₂ thin films on the R-cut and the C-cut Al₂O₃ substrates comprising compressive and tensile strains, respectively. We have identified the various insulating phases (*M1*, *M2*, and *T*) among grown films through XRD and Raman spectra. Distinct temperature-dependent electrical resistance character has been observed in these strain-mediated different insulating phases. To gain insight into the temperature-dependent SPT, we have performed the temperature-dependent Raman measurement. For probing the changes in electronic structure across IMT, temperature-dependent x-ray absorption near-edge spectroscopy (XANES) measurements have been performed across the V K edge. Our results collectively confirm that the transition in electronic structure and conductivity of these thin films occurs concomitantly and that the electronic structure is dependent largely on the nature of strain along the [001]_R axis.

II. EXPERIMENTAL DETAILS

A KrF excimer laser ($\lambda = 248$ nm, repetition rate of 5 Hz) was focused onto a target (pressed pure and $\sim 2\%$ Cr-doped V₂O₅) with a fluence of 1.1 J/cm². The ultrasonically cleaned R-cut (01 $\bar{1}2$) and C-cut (0001) Al₂O₃ substrate was maintained at a temperature of 670 °C during the deposition. Depositions were performed in an oxygen partial pressure of 10 mtorr. With the motivation to investigate the effect of different V-V pairing arrangements on insulator-to-metal characteristics of VO₂. We have grown four VO₂ thin films (with nominal thickness ~ 90 nm) having different nature and amount of strain as described below. The first thin film is pure VO₂ on R-cut Al₂O₃ substrate (VR), the second thin film is Cr-doped VO₂ on R-cut Al₂O₃ substrate (VCR), the third thin film is pure VO₂ on C-cut Al₂O₃ substrate (VC), and the fourth thin film is Cr-doped VO₂ on C-cut Al₂O₃ substrate (VCC). Hereafter, these thin films will be referred as VR, VCR, VC, and VCC, respectively. X-ray diffraction (XRD) was carried out with a Bruker D8 x-ray diffractometer equipped with Cu K α radiation. Temperature-dependent resistivity measurements were performed in the standard four-point configuration. Temperature-dependent Raman spectra were collected in backscattering geometry using a 10 mW Ar (475 nm) laser as an excitation source coupled with a Labram-HRF micro-Raman spectrometer equipped with a 50 \times objective. Temperature-dependent XANES across the V K edges was measured at beamline P64, PETRA III, DESY, Hamburg, Germany, in fluorescence mode [31]. A vanadium metal foil was used as a reference for the purpose of energy calibration.

III. RESULTS AND DISCUSSION

Figure 1(a) shows θ - 2θ XRD patterns of all four VO₂ thin films deposited under identical conditions. The diffraction peak observed at $2\theta \sim 37.17^\circ$ and $\sim 37.09^\circ$ for VR and VCR corresponds to the (200) reflection of the *M1* phase (PCPDFWIN [820661]) and (021) reflection of the *T* phase (PCPDFWIN [760674]), respectively. In VR film, the 2θ peak position has shifted to higher 2θ values compared to bulk VO₂ (marked with dashed line), which exhibits $\sim 0.19\%$ compressive strain along the a_M axis which is equivalent to the c_R axis. However, in VCR film, Cr doping has induced extra strain, and the excess strain has been compensated by stabilization of the *T* phase. The VO₂ thin films grown on C-cut Al₂O₃ substrates, VC and VCC, show the diffraction peak at $\sim 39.97^\circ$ and at $\sim 39.95^\circ$, which correspond to (020) reflection of the *M1* phase (PCPDFWIN [820661]) and (002) reflection of the *T* phase (PCPDFWIN [760674]), respectively. In VC film, the 2θ peak position has shifted to a higher 2θ value, which indicates $\sim 0.68\%$ compressive strain along the b_M axis. Similar to VCR, due to Cr doping the *T* phase has stabilized in VCC film. Zoomed-in views of the reflections of VO₂ film are shown in Fig. 1(b).

Vanadium ions dimerize and tilt in equivalent chains along the rutile c_R axis in the *M1* ($P2_1/c$) phase. In the *M2* ($C2/m$) phase, there are two types of vanadium chains; in the first chain, vanadium ions pair but do not tilt, while in the second chain, vanadium ions tilt but do not pair [20]. The *T* phase can be thought of as an intermediate phase between the *M2* and *M1* phases, where the chains become equivalent in *M1*. In contrast to the *M1* phase, the *T* ($C\bar{1}$) phase has two types of inequivalent vanadium chains (or sublattices) in which the vanadium ions are paired and tilted to different degrees [20,23,25]. XRD cannot distinguish accurately between the above discussed insulating phases due to the minor changes in the crystal structure. The thin film nature of samples makes it even more complicated to make a clear distinction between the *T* and *M2* phase from the x-ray diffraction data. Earlier reports suggest that the Raman measurement can be utilized as a tool for unambiguously characterizing the different insulating phases of VO₂ [26,33–35]. According to group theory, the *M1* phase of VO₂ has 18 Raman active modes ($9A_g$ and $9B_g$). For the *T* and *M2* phases, group theory predicts the same number of the Raman active phonon modes as the *M1* phase but with different symmetries ($10A_g + 8B_g$) [32,36,37].

Figure 1(c) shows the room temperature Raman spectra of the VO₂ thin films with the phonon modes belonging to the *M1* and *T* structures. Raman spectra of films VR and VC is in good agreement with previously published data [26,32,36,37]. A total of 13 Raman active modes at ~ 140 , ~ 195 , ~ 224 , ~ 262 , ~ 310 , ~ 337 , ~ 389 , ~ 442 , ~ 496 , ~ 582 , ~ 613 , ~ 657 cm⁻¹, and ~ 753 cm⁻¹ have been identified in the *M1* phase. Isotopic substitution and density functional theory calculations have assigned the low-frequency A_g phonons $\omega_{v,1}$ (193 cm⁻¹) and $\omega_{v,2}$ (223 cm⁻¹) to V-V dimers [Fig. 1(d)]. All the other distinguishable peaks are related to V-O vibrations. The peak ω_o at ~ 615 cm⁻¹ is a fingerprint of the VO₂ insulating phases (*M2* and *T*) [33,38]. Similar peak patterns have been observed for VCR and VCC films where the *T* phase has

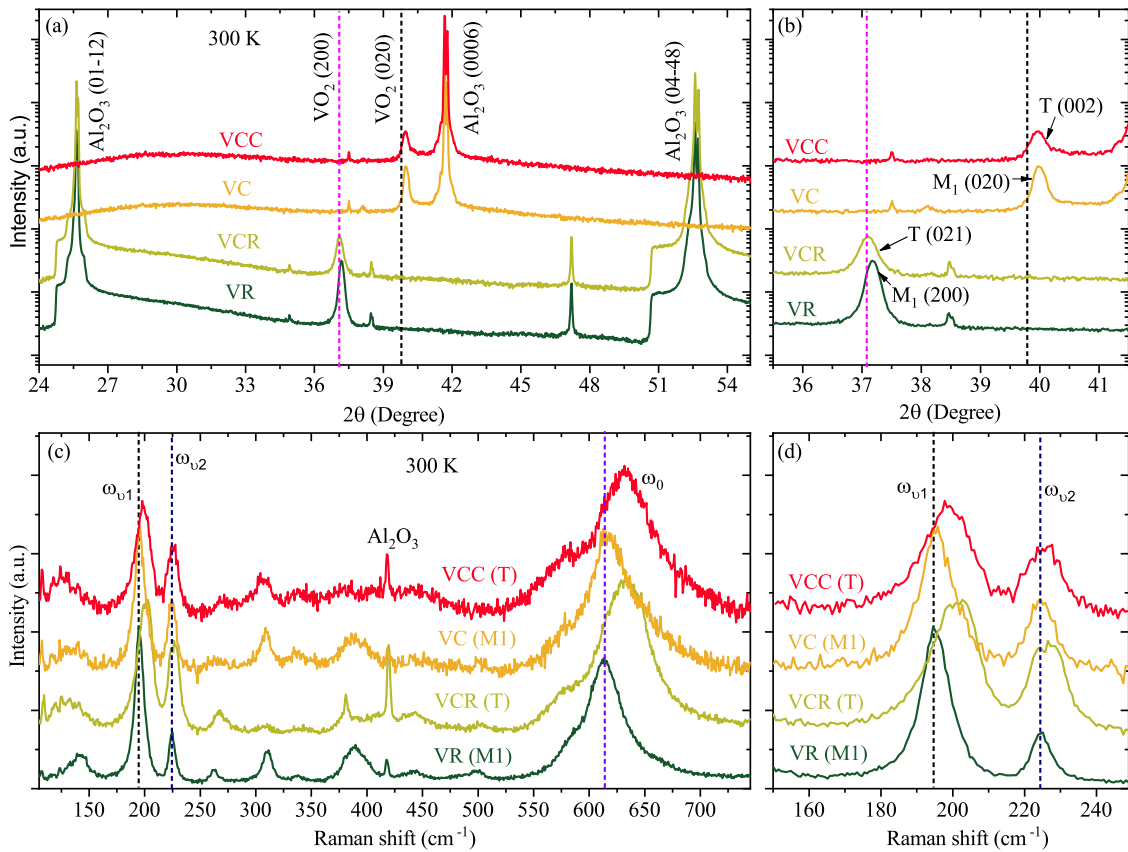


FIG. 1. (a) Room temperature θ - 2θ XRD patterns of VO₂ thin films, VR, VCR, VC, and VCC. (b) Zoomed view of the reflections of VO₂ thin films. (c) Room temperature Raman spectra of the VO₂ thin films where ω_{v1} and ω_{v2} modes correspond to V-V vibration and ω_o mode corresponds to V-O mode [32]. (d) Zoomed view of ω_{v1} and ω_{v2} Raman mode of the VO₂ films.

been stabilized but with a slight shift in the peak position of the ω_o mode from $\sim 615 \text{ cm}^{-1}$ to $\sim 633 \text{ cm}^{-1}$ [22,26,32,39], which is a characteristic of the T phase.

Figure 2 shows the temperature-dependent four-point probe resistivity measurements of the VO₂ thin films. All the four films undergo a first-order insulator-to-metal transition as evidenced by accompanying hysteresis in resistivity changes in heating and cooling cycles. We have also plotted the derivative of $\log R$ with respect to the temperature; see the inset of Fig. 2. Thin film VR exhibits an IMT temperature at $\sim 59.8^\circ\text{C}$, while (Cr-doped) film VCR exhibits an insulator-to-insulator transition at $\sim 54.6^\circ\text{C}$ and the insulator-to-metal transition near $\sim 57.8^\circ\text{C}$. The observation of these phase transitions is well supported by the literature [20,25,26,40]. Thin film VC exhibits IMT temperature at $\sim 69.1^\circ\text{C}$, while (Cr doped) film VCC shows IMT temperature at $\sim 69.5^\circ\text{C}$. Notably, the T phase has been stabilized in VCC, so we expected two transitions, similar to VCR, but we have observed only one transition. Film VR and VCR exhibits insulator-to-metal transition at lower temperatures compared to the bulk VO₂ ($\sim 67^\circ\text{C}$) [3] due to the compressive strain along the c_R axis ($\approx a_M$). Interestingly, only $\sim 0.19\%$ compressive strain along the c_R axis is found to be sufficient to lower the IMT temperature by $\sim 10^\circ\text{C}$. This observation highlights that by applying a compressive strain of $\sim 0.8\%$ along the c_R axis one can bring down the IMT temperature to the room temperature, which will be extremely useful for several potentially important

room temperature applications such as thermochromic smart windows etc. Further lowering of the IMT temperature in VCR film, due to the Cr doping-induced strain (in addition to

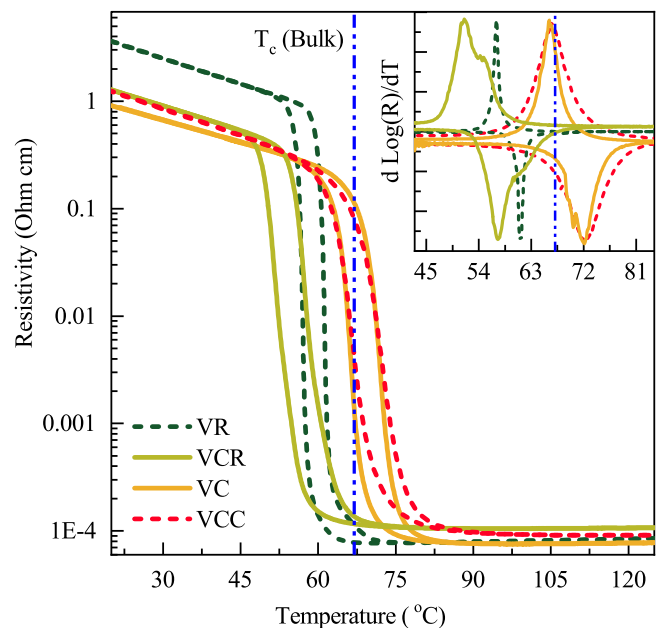


FIG. 2. Temperature-dependent resistivity of the VO₂ thin films. Inset: First derivative of resistivity with respect to temperature.

TABLE I. Lattice parameters of the thin film along the surface normal and corresponding strain present in the thin films.

Film	Lattice constant (\AA)	Strain (%)
VR	5.7414 (a_{M1})	-0.19
VC	4.4952 (b_{M1})	-0.68

the substrate-induced strain), can be seen in Fig. 2. Thin films VC and VCC exhibit the IMT at slightly higher temperature than in the bulk VO₂ (see Fig. 2). Here note that in films VC and VCC there is a compressive strain ($\sim 0.68\%$) along the b_{M1} axis induced by C-cut Al₂O₃ substrate. The c_R axis (equivalent to the a_M axis) consequently will have tensile strain (Poisson effect) in VC and VCC films. Therefore, shift of IMT temperature to a higher temperature is attributed to tensile strain in the c_R axis [29], although IMT temperature in VO₂ is reported to be sensitive to the stoichiometry, defects, crystalline quality, and doping [41–45]. However, in the present study all the films are grown under identical conditions, therefore, substrate-induced strain and Cr doping will be the major factor in the decrease/increase of the transition temperature, while other factors will play a minimal role. Further, when the temperature is varied, the mismatch in thermal expansion may result in the change in strain. The thermal expansion coefficient of the different axis of Al₂O₃ is found to be almost similar $\sim 4.5\text{--}5.3 \times 10^{-6}/^\circ\text{C}$ [46], so we believe that there would not be a significant difference in the contribution from R- and C-cut Al₂O₃ during IMT in VO₂, while, upon cooling from the growth temperature, tensile/compressive strain is stored in the films as a consequence of mismatch of the lattice parameters between VO₂ and different cuts of the sapphire substrates [46–49]. Moreover, observed relative shifts in the IMT temperature are well supported by our expectations, which is also consistent with the strain present in the c_R axis [28]. Lattice constants of the thin films (VR and VC) along the surface normal and corresponding strain are shown in Table I, and crystallographical details of all the thin films at room temperature and obtained transition temperatures are tabulated in Table II.

To track the structural phase transition path followed by these strain-mediated insulating phases, Raman spectroscopy was carried out as a function of temperature. Measurements presented here are from the cooling cycles, and similar behavior is expected in the heating cycles except that transition temperatures will appear at slightly higher temperature due to the first-order nature of the transition. With the increase of temperature [see Fig. 3(a)] peak intensity in the Raman spectrum becomes weaker and finally disappears, which corresponds to a structural transition from the monoclinic *MI*

structure to the rutile *R* structure. The Cr-doped VO₂ thin film (VCR) has an intermediate Mott monoclinic *M2* structure between the room temperature *T* structure and the high-temperature rutile *R* structure, as evidenced by a blueshift in the position of the ω_o vibration from room temperature to intermediate temperature, as shown in Fig. 3(b) [32,33,38,39]. Temperature-dependent Raman spectra of VC and VCC can be seen in Figs. 3(c) and 3(d), respectively.

To further evaluate the temperature-dependent structural rearrangement, we have plotted the temperature-dependent Raman shift and FWHM of the Raman frequency ω_o (obtained by Lorentzian fitting of the phonon modes across ω_o ($\sim 615 \text{ cm}^{-1}$) from the data in the cooling cycle in Figs. 3(e) and 3(f), respectively). It is to be noted that this broad Raman peak consists of three modes (~ 582 , ~ 615 , and $\sim 657 \text{ cm}^{-1}$). The monoclinic *MI*, *M2*, and triclinic *T* structures of VO₂ differ in the arrangement of the vanadium atoms along the c_R axis. Obtained variation in Raman shift with temperature clearly signifies that in film VR, where the *MI* phase has been observed, no blueshifting in the ω_o mode has been observed; only a slight softening can be observed at higher temperatures, which is a clear indication that the *MI* phase transforms directly into the *R* phase with increasing temperature and matches well with earlier reports [50,51]. However, VCR film where *T* phase is observed has an intermediate monoclinic *M2* structure between room temperature and high-temperature rutile structure, as evidenced by a blueshift in the ω_o mode from $\sim 630 \text{ cm}^{-1}$ to $\sim 634 \text{ cm}^{-1}$ [23,26]. Although, in film VC, *MI* phase has been stabilized at room temperature, but the blueshift in the ω_o mode, from $\sim 618.5 \text{ cm}^{-1}$ to $\sim 619.5 \text{ cm}^{-1}$, can be observed with increasing temperature, which is well in agreement with earlier reports [21,33]. This clearly indicates that unlike film VR, in film VC the transformation of the *MI* phase to the *R* phase happens through the intermediate *M2* phase. Similar to the film VCR, film VCC also transforms from *T* to *M2* to *R* phase, signified by the blueshift in the ω_o mode. The FWHM of each mode can be seen increasing with rising temperature of all the films, which is usual [see Fig. 3(f)]. Temperature evolution of structural phases with temperature in these films is summarized in Table III.

Structural transition in VO₂ is accompanied with changes in the electronic band structure around the Fermi level (E_F), which can be qualitatively understood within a crystal-field model [53]. The *3d* electronic levels of the V ions in an octahedral environment are crystal-field split into a combination of triply degenerate low-energy t_{2g} states and doubly degenerate high-energy e_g^* states. The small orthorhombic component of the crystal field associated with the different equatorial and apical V–O distances in an octahedral environment further separates the t_{2g} orbitals into a single

TABLE II. Crystallographical details of the thin films.

Film	Crystal system	Space group	Orientation [hkl]	Transition temperature
VO ₂ on R-cut Al ₂ O ₃ (VR)	Monoclinic (<i>M1</i>)	P2 ₁ /C	[200]	$\sim 59.8^\circ$
Cr VO ₂ on R-cut Al ₂ O ₃ (VCR)	Triclinic (<i>T</i>)	C $\bar{1}$	[021]	$\sim 54.6^\circ$
VO ₂ on C-cut Al ₂ O ₃ (VC)	Monoclinic (<i>M1</i>)	P2 ₁ /C	[020]	$\sim 69.^\circ$
Cr VO ₂ on C-cut Al ₂ O ₃ (VCC)	Triclinic (<i>T</i>)	C $\bar{1}$	[002]	$\sim 69.4^\circ$

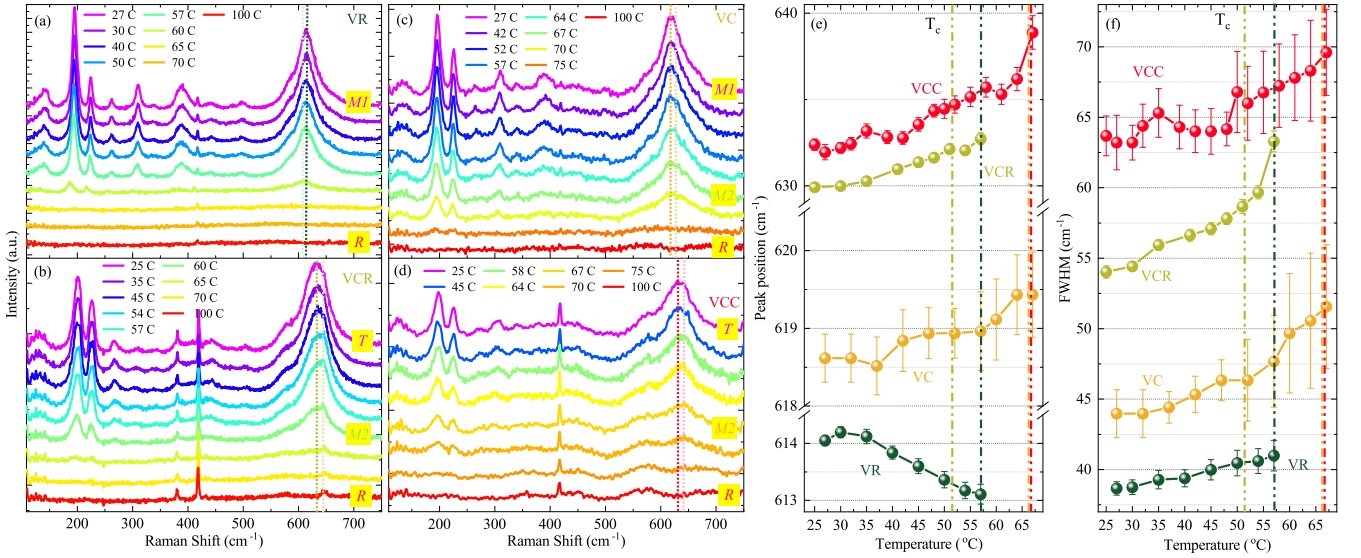


FIG. 3. Temperature-dependent Raman spectra of VO₂ thin films (a) VR, (b) VCR, (c) VC, and (d) VCC. (e) Raman shift and (f) FWHM variations with temperature of ω_o mode (615 cm^{-1}).

a_{1g} ($d_{||}$) orbital and doubly degenerate e_g^π orbitals. The e_g^σ and the e_g^π states hybridize with the O $2p$ orbitals to form σ bonding, σ^* antibonding molecular, and π bonding and π^* antibonding molecular orbitals, respectively. The a_{1g} orbitals are directed parallel to the rutile c axis (c_R) [53]. In the metallic state density of states at the E_F is due to mixture of the a_{1g} orbitals and antibonding e_g^π orbitals (π^*). Across the metal-to-insulator transition, dimerization of the V ions along the c_R splits the highly directional a_{1g} orbitals that mediate V–V bonds into a bonding and an antibonding combination [see the band diagram in Fig. 4(d)]. XANES corresponds to electronic transitions from deep levels to empty states near the Fermi level of the selected elements in a system. XANES at a transition metal K edge reflects the local density of states (LDOS) of the metal $3d$ orbitals and the local structural properties of neighboring atoms around the transition metal ion [6]. Strain present in the thin film due to the Cr doping and substrate can affect the V $3d$ orbital occupation across the Fermi level. The pre-edge features correspond to a V $1s$ to $3d$ dipole forbidden transition which becomes allowed due to overlapping of the V $3d$ orbitals with the V $4p$ and O $2p$ orbitals, while the main absorption edge (D and E) represents the V $1s$ to $4p$ dipole allowed transitions [6,26,30]. The XANES spectra show a valence state of V⁴⁺ [see Fig. 4(a)]. The pre-edge feature contains two features corresponding to the crystal-field split V $3d$ state, i.e., t_{2g} and e_g [see Fig. 4(b)] [52]. Figure 4(c) shows normalized intensity of the pre-edge features at various temperatures during heating.

TABLE III. Summary of temperature-induced phase evolution of the thin films with increasing temperature.

VR →	M1 to R
VCR →	T to M2 to R
VC →	M1 to M2 to R
VCC →	T to M2 to R

The area under the pre-edge features is directly proportional to density of states of the V $3d$ orbitals, which is strongly affected by the first and second nearest-neighboring atoms [6,54,55]. Hence, the pre-edge peak intensity is highly sensitive to the local geometrical structure around the absorbing atom (V). The pre-edge features become less intense and broader above the IMT temperature as shown in Fig. 4(c). The quantitative spectral changes in the pre-edge features across the IMT were

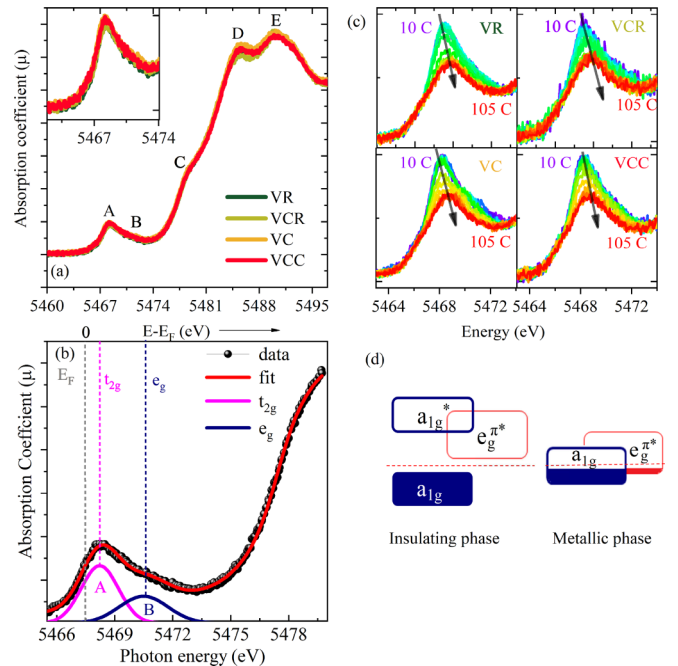


FIG. 4. (a) Room temperature XANES spectra of VO₂ thin films, which resemble each other. Inset: Zoomed view of pre-edge feature. (b) Fitted pre-edge features (at room temperature) and compared with crystal-field split t_{2g} and e_g features of VO₂ [52]. (c) Temperature dependence of pre-edge feature of VO₂ thin films. (d) VO₂ band diagrams across the Fermi level, in insulating and metallic states.

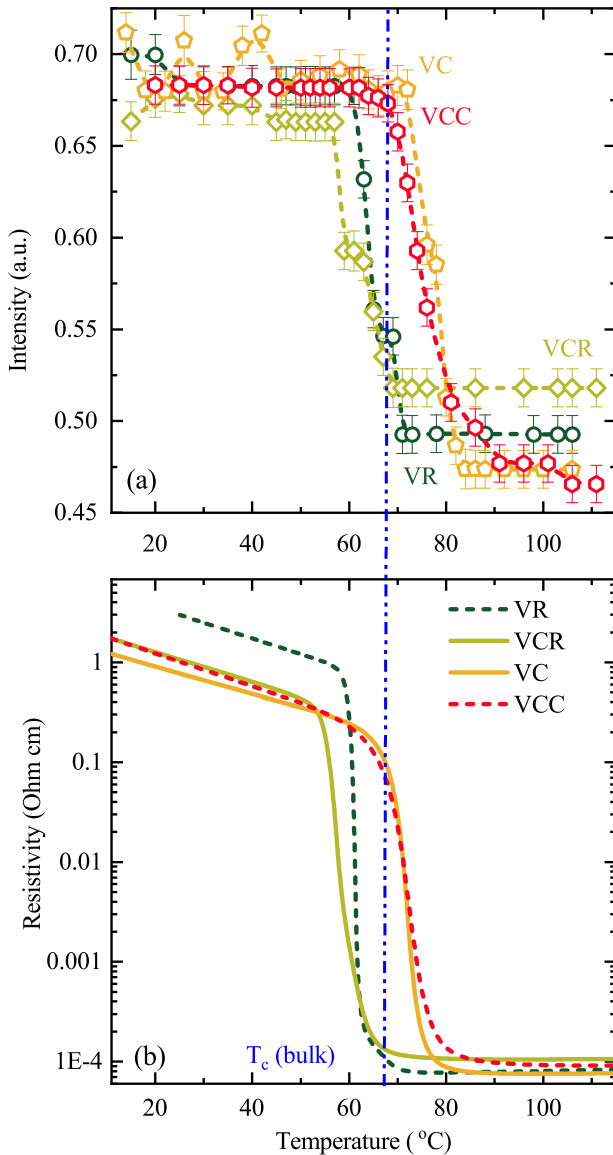


FIG. 5. (a) XANES pre-edge peak intensity variation with temperature. (b) Resistivity as a function of temperature. Both ((a) & (b)) plots are for heating cycles.

determined by fitting with an arctangent-pseudo-Voigt model [Fig. 4(b)]. The intensity of the pre-edge features in all the thin films overlaps very well (see inset of the Fig. 4(a)) which confirms the similar electronic structure in the $M1$ and T insulating phases of VO_2 around the Fermi level.

The energy separation among the t_{2g} and e_g features of the pre-edge peak correspond to the crystal-field splitting energy, which is sensitive to the V-O apical bond length [53,56]. At room temperature, the energy position of t_{2g} and e_g is separated by ~ 2.3 eV, ~ 2.51 eV, ~ 1.8 eV, and ~ 1.86 eV for the films VR, VCR, VC, and VCC, respectively. A considerable difference in the energy separation between t_{2g} and e_g bands has been observed in the films having a different nature of strain, i.e., compressive and tensile strain along the c_R axis. Figure 5(a) shows the temperature-dependent intensity variation of the pre-edge spectral features of all the thin films across IMT temperature. A sharp pre-edge intensity change

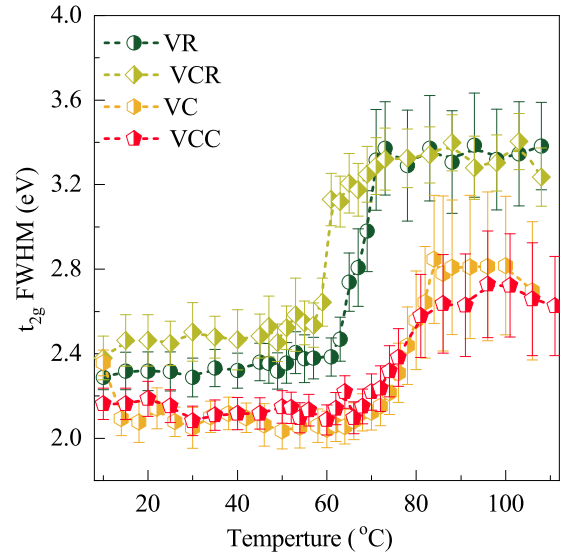


FIG. 6. FWHM of the peak A (t_{2g}) in Fig. 4(b) with varying temperature.

has been observed in the VR thin film compared to the broader transition in VCR, VC, and VCC thin films, which can be ascribed to the presence of the VO_2 $M2$ phase at intermediate temperatures between the room-temperature insulating phase and the high-temperature metallic phase in the VCR, VC, and VCC thin films. The pre-edge intensity change across the IMT can be explained in terms of local structural changes happening around the V atom. The intensity of the pre-edge spectral features is directly proportional to the distortion in the V-O octahedron. In VO_2 , a V-O octahedron consists of one central V atom and six O atoms as the nearest neighbors of the V atom. In the $M1$, $M2$, and T phases the V-O octahedron has a distorted form with different bond lengths and tilted angles of the six V-O pairs [25,26] while the metallic R phase has less distorted octahedron. The lower pre-edge intensity in the metallic phase can also be ascribed to the higher occupancy of the V $3d$ states around the Fermi level, compared to the insulating phases [see Fig. 4(d)] [6,54,57,58].

The transition temperatures obtained from the pre-edge peak intensity variation matches very well the resistivity data [see Fig. 5(b)], within a slight variation, which is inevitable in two different sets of measurements. The relative shift of the transition temperatures for different VO_2 thin films obtained from the XANES measurements correlates very well with the values obtained from the resistivity measurements. Our observations clearly indicate that the electronic structure changes in the VO_2 thin films across the IMT, possessing compressive and tensile strain, match very well the resistivity measurements and confirm that the strain in the thin films is the main driving force for controlling the IMT properties.

Figure 6 exhibits variation in the FWHM of the pre-edge feature A (t_{2g}) across the IMT in all the thin films. One can clearly observe that in all the films FWHM is increasing with increasing temperature and undergoes an abrupt increase around the IMT temperatures, which can be explained in terms of the $d_{||}$ multiple final-state configurations in the metallic state. The low-temperature insulating phase has only the $d_{||}^1$ final-state configuration, while in the metallic phase there

can be the possibility of three components, which are characterized by different occupation numbers of the d_{\parallel} band, i.e., d_{\parallel}^2 , d_{\parallel}^1 , and d_{\parallel}^0 [52,59]. The smaller magnitude of the FWHM variation around the IMT temperatures in the case of VC and VCC films can be attributed to the presence of tensile strain along the c_R axis, which will result in the decrease of the V-O apical bond length, consistent with the earlier study by Aetukuri *et al.* [29]. The decrease in apical V-O bond length will result in an increase in the p - d overlap, which will push the π^* states to higher energy, and as a result of the higher shift of the π^* states, the probability of the d_{\parallel}^0 final state configuration will be reduced. Hence, in that scenario, only the d_{\parallel}^1 and the d_{\parallel}^2 configurations will contribute to the FWHM of the pre-edge feature in the metallic state. Our FWHM vs T results also confirm that the nature of the strain in the thin films is dictating the electronic structure behavior across the IMT. In the end, it is to be highlighted that earlier reports suggest that the Cr-doped VO₂ exhibits almost similar behavior as obtained under the uniaxial strain along the $[110]_R$ direction [22]. Here we have attempted to modify the electronic structure by the application of strain along the $[001]_R$ (c_R) axis (substrate induced) as well as along the $[110]_R$ direction (by Cr doping). Our room temperature XANES spectra of all the thin films are overlapping [see Fig. 4(a)], which suggests similar electronic structure of $M1$ (VR and VC) and T (VCR and VCC) phases of VO₂. Further, the intensity of the pre-edge feature of XANES spectra strongly resembles the IMT characteristics obtained by electrical transport measurements [see Figs. 5(a) and 5(b)]. This suggests that although they have a similar electronic structure, IMT transition is largely determining by the nature of the strain. Compared to bulk, IMT temperature in compressive strained VO₂ film along the c_R axis has decreased, while in tensile strained VO₂ film along the c_R axis the transition temperature has shifted towards higher temperature. On the Cr doping, different effects are observed in differently strained conditions, i.e., IMT temperature further lowers in compressive strained film along the c_R ($\approx a_{M1}$) axis, while transition temperature is almost insensitive when Cr is doped in tensile strained film along the c_R axis. Although the Cr doping has some significant impact on determining the IMT temperature, it is playing a minimal role in electronic structure modifications (it stabilizes the other insulating phases of almost similar electronic structure).

IV. CONCLUSIONS

In conclusion, to investigate the effect of distinct V-V dimers (which play a critical role in determining the IMT

temperature in VO₂) on the IMT, we have stabilized different insulating phases $M1$, $M2$, and T by utilizing different natures (compressive/tensile) of strain along the c_R axis and by Cr doping. The intermediate $M2$ phase was accessed at intermediate temperatures while heating in pure (having tensile strain along c_R axis in the $M1$ phase) and Cr-doped (T phase) VO₂ thin films. Compressive strain along the rutile c_R axis has lowered the transition temperature compared to bulk VO₂, while tensile strain along the c_R axis has shifted the transition temperature to a higher temperature. We have successfully tracked the exact structural phase transformation path followed by the different insulating phases by utilizing the temperature-dependent Raman spectroscopy. Film where the c_R axis has compressive strain exhibits the transition from $M1$ phase to the R phase directly, while the thin films, which have stabilized the T phase at room temperature, transforms to the R phase via the $M2$ phase with increasing temperature. Our results also show that due to the presence of tensile strain along the c_R axis, the $M1$ phase can also adopt the $M2$ phase when transforming to the R phase, while generally the $M1$ phase goes to the R phase directly. IMT temperature obtained by temperature-dependent integrated intensity of the pre-edge features (combined t_{2g} and e_g bands) has been found to scale directly with resistivity data. Our results clearly confirm that electronic structure and IMT temperature are dictated largely by the nature of strain, i.e., compressive or tensile strain along the $[001]_R$ axis, while they are least affected by the different insulating phases. Finally, the current study establishes the procedure of using strain as a control parameter to tune the IMT in VO₂, which is essential for technological applications.

ACKNOWLEDGMENTS

The authors acknowledge DESY (Hamburg, Germany), a member of the Helmholtz Association HGF, for the provision of experimental facilities. Part of this research were carried at PETRA III, and we would like to thank Aleksandr Kalinko, Akhil Tayal, Maria Naumova, and Wolfgang Caliebe for assistance in using XAFS-beamline P64. The authors also acknowledge the support from the India-DESY collaboration for beamtime allocation for Proposal No. I-2020852. S.S.M. acknowledges the financial support from SERB, India, in the form of the national postdoctoral fellowship (NPDF) award (PDF/2021/002137). H.L. acknowledges the support by the Learning & Academic research institution for Master's and Ph.D. students and the Postdocs (LAMP) Program of the National Research Foundation of Korea (NRF) grant funded by the Ministry of Education (No. RS-2023-00285390).

-
- [1] M. Imada, A. Fujimori, and Y. Tokura, Metal-insulator transitions, *Rev. Mod. Phys.* **70**, 1039 (1998).
 - [2] A. Zylbersztein and N. F. Mott, Metal-insulator transition in vanadium dioxide, *Phys. Rev. B* **11**, 4383 (1975).
 - [3] F. Morin, Oxides which show a metal-to-insulator transition at the Neel temperature, *Phys. Rev. Lett.* **3**, 34 (1959).
 - [4] M. M. Qazilbash, M. Brehm, B.-G. Chae, P.-C. Ho, G. O. Andreev, B.-J. Kim, S. J. Yun, A. Balatsky, M. Maple,

F. Keilmann *et al.*, Mott transition in VO₂ revealed by infrared spectroscopy and nano-imaging, *Science* **318**, 1750 (2007).

- [5] Z. Shao, X. Cao, H. Luo, and P. Jin, Recent progress in the phase-transition mechanism and modulation of vanadium dioxide materials, *NPG Asia Mater.* **10**, 581 (2018).
- [6] I.-H. Hwang, Z. Jin, C.-I. Park, and S.-W. Han, The influence of structural disorder and phonon on metal-to-insulator transition of VO₂, *Sci. Rep.* **7**, 14802 (2017).

- [7] M. Liu, H. Y. Hwang, H. Tao, A. C. Strikwerda, K. Fan, G. R. Keiser, A. J. Sternbach, K. G. West, S. Kittiwatanakul, J. Lu *et al.*, Terahertz-field-induced insulator-to-metal transition in vanadium dioxide metamaterial, *Nature (London)* **487**, 345 (2012).
- [8] S. S. Majid, S. R. Sahu, A. Ahad, K. Dey, K. Gautam, F. Rahman, P. Behera, U. Deshpande, V. G. Sathe, and D. K. Shukla, Role of V-V dimerization in the insulator-metal transition and optical transmittance of pure and doped VO₂ thin films, *Phys. Rev. B* **101**, 014108 (2020).
- [9] L. Chen, Y. Cui, H. Luo, and Y. Gao, Atomic and electronic structures of charge-doping VO₂: First-principles calculations, *RSC Adv.* **10**, 18543 (2020).
- [10] Y. H. Matsuda, D. Nakamura, A. Ikeda, S. Takeyama, Y. Suga, H. Nakahara, and Y. Muraoka, Magnetic-field-induced insulator-metal transition in W-doped VO₂ at 500 t, *Nat. Commun.* **11**, 3591 (2020).
- [11] X. He, N. Punpongjareorn, W. Liang, Y. Lin, C. Chen, A. J. Jacobson, and D.-S. Yang, Photoinduced strain release and phase transition dynamics of solid-supported ultrathin vanadium dioxide, *Sci. Rep.* **7**, 10045 (2017).
- [12] H.-T. Kim, B.-G. Chae, D.-H. Youn, S.-L. Maeng, G. Kim, K.-Y. Kang, and Y.-S. Lim, Mechanism and observation of mott transition in VO₂-based two-and three-terminal devices, *New J. Phys.* **6**, 52 (2004).
- [13] N. Shukla, A. V. Thathachary, A. Agrawal, H. Paik, A. Aziz, D. G. Schlom, S. K. Gupta, R. Engel-Herbert, and S. Datta, A steep-slope transistor based on abrupt electronic phase transition, *Nat. Commun.* **6**, 7812 (2015).
- [14] J. Zhou, Y. Gao, Z. Zhang, H. Luo, C. Cao, Z. Chen, L. Dai, and X. Liu, VO₂ thermochromic smart window for energy savings and generation, *Sci. Rep.* **3**, 3029 (2013).
- [15] S. Liang, Q. Shi, H. Zhu, B. Peng, and W. Huang, One-step hydrothermal synthesis of W-doped VO₂ (m) nanorods with a tunable phase-transition temperature for infrared smart windows, *ACS Omega* **1**, 1139 (2016).
- [16] E. Strelcov, Y. Lilach, and A. Kolmakov, Gas sensor based on metal-insulator transition in VO₂ nanowire thermistor, *Nano Lett.* **9**, 2322 (2009).
- [17] C. V. S. Reddy, E. H. Walker Jr, S. Wicker Sr, Q. L. Williams, and R. R. Kalluru, Synthesis of VO₂ (b) nanorods for Li battery application, *Curr. Appl. Phys.* **9**, 1195 (2009).
- [18] I. Mjejri, N. Etteyeb, and F. Sediri, Mesoporous vanadium oxide nanostructures: Hydrothermal synthesis, optical and electrochemical properties, *Ceram. Int.* **40**, 1387 (2014).
- [19] F. Cilento, C. Giannetti, G. Ferrini, S. Dal Conte, T. Sala, G. Coslovich, M. Rini, A. Cavalleri, and F. Parmigiani, Ultrafast insulator-to-metal phase transition as a switch to measure the spectrogram of a super-continuum light pulse, *Appl. Phys. Lett.* **96**, 021102 (2010).
- [20] J. P. Pouget, H. Launois, T. M. Rice, P. Dernier, A. Gossard, G. Villeneuve, and P. Hagenmuller, Dimerization of a linear Heisenberg chain in the insulating phases of V_{1-x}Cr_xO₂, *Phys. Rev. B* **10**, 1801 (1974).
- [21] J. H. Park, J. M. Coy, T. S. Kasirga, C. Huang, Z. Fei, S. Hunter, and D. H. Cobden, Measurement of a solid-state triple point at the metal-insulator transition in VO₂, *Nature (London)* **500**, 431 (2013).
- [22] J. Pouget, H. Launois, J. D'haenens, P. Merenda, and T. Rice, Electron localization induced by uniaxial stress in pure VO₂, *Phys. Rev. Lett.* **35**, 873 (1975).
- [23] M. Ghedira, H. Vincent, M. Marezio, and J. Launay, Structural aspects of the metal-insulator transitions in V_{0.985}Al_{0.015}O₂, *J. Solid State Chem.* **22**, 423 (1977).
- [24] M. Marezio, D. B. McWhan, J. Remeika, and P. Dernier, Structural aspects of the metal-insulator transitions in Cr-doped VO₂, *Phys. Rev. B* **5**, 2541 (1972).
- [25] T. J. Huffman, C. Hendriks, E. J. Walter, J. Yoon, H. Ju, R. Smith, G. L. Carr, H. Krakauer, and M. M. Qazilbash, Insulating phases of vanadium dioxide are Mott-Hubbard insulators, *Phys. Rev. B* **95**, 075125 (2017).
- [26] S. S. Majid, D. K. Shukla, F. Rahman, S. Khan, K. Gautam, A. Ahad, S. Francoual, R. Choudhary, V. G. Sathe, and J. Stremper, Insulator-metal transitions in the T phase Cr-doped and M1 phase undoped VO₂ thin films, *Phys. Rev. B* **98**, 075152 (2018).
- [27] T. J. Huffman, P. Xu, A. J. Hollingshad, M. M. Qazilbash, L. Wang, R. A. Lukaszew, S. Kittiwatanakul, J. Lu, and S. A. Wolf, Modification of electronic structure in compressively strained vanadium dioxide films, *Phys. Rev. B* **91**, 205140 (2015).
- [28] Y. Muraoka and Z. Hiroi, Metal-insulator transition of VO₂ thin films grown on TiO₂ (001) and (110) substrates, *Appl. Phys. Lett.* **80**, 583 (2002).
- [29] N. B. Aetukuri, A. X. Gray, M. Drouard, M. Cossale, L. Gao, A. H. Reid, R. Kukreja, H. Ohldag, C. A. Jenkins, E. Arenholz *et al.*, Control of the metal-insulator transition in vanadium dioxide by modifying orbital occupancy, *Nat. Phys.* **9**, 661 (2013).
- [30] I.-H. Hwang, C.-I. Park, S. Yeo, C.-J. Sun, and S.-W. Han, Decoupling the metal insulator transition and crystal field effects of VO₂, *Sci. Rep.* **11**, 3135 (2021).
- [31] W. Caliebe, V. Murzin, A. Kalinko, and M. Görlitz, High-flux XAFS-beamline p64 at PETRA III, *AIP Conf. Proc.* **2054**, 060031 (2019).
- [32] C. Marini, E. Arcangeletti, D. Di Castro, L. Baldassare, A. Perucchi, S. Lupi, L. Malavasi, L. Boeri, E. Pomjakushina, K. Conder *et al.*, Optical properties of V_{1-x}Cr_xO₂ compounds under high pressure, *Phys. Rev. B* **77**, 235111 (2008).
- [33] Y. Ji, Y. Zhang, M. Gao, Z. Yuan, Y. Xia, C. Jin, B. Tao, C. Chen, Q. Jia, and Y. Lin, Role of microstructures on the m1-m2 phase transition in epitaxial VO₂ thin films, *Sci. Rep.* **4**, 4854 (2014).
- [34] A. Tselev, I. Luk'Yanchuk, I. Ivanov, J. Budai, J. Tischler, E. Strelcov, A. Kolmakov, and S. Kalinin, Symmetry relationship and strain-induced transitions between insulating m1 and m2 and metallic r phases of vanadium dioxide, *Nano Lett.* **10**, 4409 (2010).
- [35] E. Strelcov, A. Tselev, I. Ivanov, J. D. Budai, J. Zhang, J. Z. Tischler, I. Kravchenko, S. V. Kalinin, and A. Kolmakov, Doping-based stabilization of the m2 phase in free-standing VO₂ nanostructures at room temperature, *Nano Lett.* **12**, 6198 (2012).
- [36] R. Srivastava and L. Chase, Raman spectrum of semiconducting and metallic VO₂, *Phys. Rev. Lett.* **27**, 727 (1971).
- [37] P. Schilbe and D. Maurer, Lattice dynamics in VO₂ near the metal-insulator transition, *Mater. Sci. Eng., A* **370**, 449 (2004).
- [38] K. Okimura, N. Hanis Azhan, T. Hajiri, S.-i. Kimura, M. Zaghrioui, and J. Sakai, Temperature-dependent Raman and

- ultraviolet photoelectron spectroscopy studies on phase transition behavior of VO₂ films with m1 and m2 phases, *J. Appl. Phys.* **115**, 153501 (2014).
- [39] J. M. Atkin, S. Berweger, E. K. Chavez, M. B. Raschke, J. Cao, W. Fan, and J. Wu, Strain and temperature dependence of the insulating phases of VO₂ near the metal-insulator transition, *Phys. Rev. B* **85**, 020101(R) (2012).
- [40] B. S. Mun, K. Chen, Y. Leem, C. Dejoie, N. Tamura, M. Kunz, Z. Liu, M. E. Grass, C. Park, J. Yoon *et al.*, Observation of insulating–insulating monoclinic structural transition in macro-sized VO₂ single crystals [Phys. Status Solidi RRL 5, 107 (2015)], *Phys. Status Solidi RRL* **9**, 206 (2015).
- [41] W. Brückner, W. Moldenhauer, H. Wich, E. Wolf, H. Oppermann, U. Gerlach, and W. Reichelt, The range of homogeneity of VO₂ and the influence of the composition on the physical properties. II. The change of the physical properties in the range of homogeneity, *Phys. Status Solidi A* **29**, 63 (1975).
- [42] N. Kimizuka, M. Ishii, I. Kawada, M. Saeki, and M. Nakahira, Behavior of vanadium dioxide single crystals synthesized under the various oxygen partial pressures at 1500 K, *J. Solid State Chem.* **9**, 69 (1974).
- [43] D. Fu, K. Liu, T. Tao, K. Lo, C. Cheng, B. Liu, R. Zhang, H. A. Bechtel, and J. Wu, Comprehensive study of the metal-insulator transition in pulsed laser deposited epitaxial VO₂ thin films, *J. Appl. Phys.* **113**, 043707 (2013).
- [44] W. Fan, J. Cao, J. Seidel, Y. Gu, J. W. Yim, C. Barrett, K. M. Yu, J. Ji, R. Ramesh, L. Q. Chen, J. Wu, Large kinetic asymmetry in the metal-insulator transition nucleated at localized and extended defects, *Phys. Rev. B* **83**, 235102 (2011).
- [45] K. Liu, S. Lee, S. Yang, O. Delaire, and J. Wu, Recent progresses on physics and applications of vanadium dioxide, *Mater. Today* **21**, 875 (2018).
- [46] Y. Cui and S. Ramanathan, Substrate effects on metal-insulator transition characteristics of rf-sputtered epitaxial VO₂ thin films, *J. Vac. Sci. Technol. A* **29**, 041502 (2011).
- [47] J. Sakai, M. Zaghrioui, M. Matsushima, H. Funakubo, and K. Okimura, Impact of thermal expansion of substrates on phase transition temperature of VO₂ films, *J. Appl. Phys.* **116**, 123510 (2014).
- [48] H. Koo, S. Yoon, O.-J. Kwon, K.-E. Ko, D. Shin, S.-H. Bae, S.-H. Chang, and C. Park, Effect of lattice misfit on the transition temperature of VO₂ thin film, *J. Mater. Sci.* **47**, 6397 (2012).
- [49] J. Lappalainen and M. Kangaspuoskari, Interface effects of strain-energy potentials on phase transition characteristics of VO₂ thin-films, *ACS Omega* **8**, 21083 (2023).
- [50] M. Nazari, Y. Zhao, V. V. Kuryatkov, Z. Y. Fan, A. A. Bernussi, and M. Holtz, Temperature dependence of the optical properties of VO₂ deposited on sapphire with different orientations, *Phys. Rev. B* **87**, 035142 (2013).
- [51] S. R. Sahu, S. S. Majid, A. Ahad, A. Tripathy, K. Dey, S. Pal, B. K. De, W.-P. Hsieh, R. Rawat, V. G. Sathe, and D. K. Shukla, Kinetically-decoupled electrical and structural phase transitions in VO₂, *Phys. Rev. B* **107**, 134106 (2023).
- [52] A. Bianconi, Multiplet splitting of final-state configurations in x-ray-absorption spectrum of metal VO₂: Effect of core-hole-screening, electron correlation, and metal-insulator transition, *Phys. Rev. B* **26**, 2741 (1982).
- [53] J. B. Goodenough, The two components of the crystallographic transition in VO₂, *J. Solid State Chem.* **3**, 490 (1971).
- [54] Z. Jin, I.-H. Hwang, C.-I. Park, J.-K. Son, and S.-W. Han, Synthesis and temperature-dependent local structural and electrical properties of VO₂ films, *Curr. Appl. Phys.* **16**, 183 (2016).
- [55] S. Seo, E. Jeong, C. Kwak, C. Park, Z. Jin, S. Kim, and S. Han, X-ray absorption fine structure study of cobalt ion distribution in ferromagnetic Zn_{1-x}Co_xO films, *J. Phys.: Condens. Matter* **25**, 256005 (2013).
- [56] V. Eyert, The metal-insulator transitions of VO₂: A band theoretical approach, *Annal. Phys.* **514**, 650 (2002).
- [57] T. C. Koethe, Z. Hu, M. W. Haverkort, C. Schüßler-Langeheine, F. Venturini, N. B. Brookes, O. Tjernberg, W. Reichelt, H. H. Hsieh, H.-J. Lin *et al.*, Transfer of spectral weight and symmetry across the metal-insulator transition in VO₂, *Phys. Rev. Lett.* **97**, 116402 (2006).
- [58] S. Biermann, A. Poteryaev, A. I. Lichtenstein, and A. Georges, Dynamical singlets and correlation-assisted peierls transition in VO₂, *Phys. Rev. Lett.* **94**, 026404 (2005).
- [59] C. Marini, S. Pascarelli, O. Mathon, B. Joseph, L. Malavasi, and P. Postorino, Tracking competitive lattice distortions in strongly correlated VO₂-based systems: A temperature-dependent EXAFS study, *Europhys. Lett.* **102**, 66004 (2013).